

Fiber optics in curved space-times

Thomas B. Mieling ^{1,*} and Mario Hudelist ²

¹University of Vienna, Faculty of Physics and Research Network TURIS, Boltzmannngasse 5, 1090 Vienna, Austria

²University of Vienna, Faculty of Physics, Boltzmannngasse 5, 1090 Vienna, Austria

(Dated: February 17, 2025)

Single-mode fibers are used in fiber-optic gyroscopes to measure the Sagnac effect and are planned to be used in forthcoming experiments on the gravitationally induced phase shift in single photons. However, current theoretical models of such experiments are limited to ray-optics approximations or, if based on wave optics, to a restricted class of fiber alignments. To overcome these shortcomings, this paper develops a comprehensive perturbative scheme to solve for electromagnetic modes, i.e., monochromatic solutions to Maxwell's equations, of arbitrarily bent step-index fibers in general stationary space-times. This leads to transport equations for the electromagnetic phase and polarization that include the gravitational redshift, the Sagnac effect, a generalization of Rytov's law to curved space, a gravitational Faraday effect in the form of shift-induced gyrotropy, as well as inverse spin Hall effects caused by fiber bending, gravitational acceleration, and space-time curvature.

I. INTRODUCTION

Optical fibers are essential to telecommunication, but also to sensing applications and state-of-the-art quantum optics experiments [1–3]. The latter include interferometric measurements of rotational effects in light-propagation, such as fiber-optic gyroscopes [4] and multi-photon Sagnac interferometers [5–7], as well as forthcoming tests of the gravitational redshift of single photons and entangled photon pairs in Mach–Zehnder interferometers [8, 9].

Current theoretical models of fiber optics in non-inertial systems and, more generally, curved space-times (to describe gravitational effects using the framework of general relativity) are limited to either strongly simplified models of light propagation or highly restrictive assumptions on the fiber geometry. Indeed, the vast majority of theoretical models of the Sagnac effect and the gravitational redshift are based on geometrical optics [10–13]. While such models allow for arbitrary fiber geometries, their application to commonly used single-mode fibers (SMF) is questionable because ray optics is ill-suited for their description even in flat space-time [1, p. 23]. This has motivated the development of more rigorous models based on Maxwell's equations and their generalization to curved space-times, but due to the complexity of these equations they were successfully applied only to special fiber geometries. For example, Ref. [14] computed the Sagnac effect in planar fiber loops (using a Gaussian approximation of the transverse field profile, thereby avoiding mathematical complications arising from discontinuities in the SMF's index profile) and Ref. [15] gave a solution for straight fibers (without Gaussian approximations). Similarly, rigorous analyses of the gravitational redshift in SMF are currently limited to straight fibers at constant gravitational potentials in post-Newtonian metrics [16, 17], while

experimental proposals suggest using fiber-optic spools instead [8]. Likewise, current theoretical models of optical solitons in the Schwarzschild geometry are limited to a small set of fiber alignments [18, 19].

Recent theory developments allow overcoming these limitations of fiber-optics calculations. Specifically, Ref. [20] developed a perturbative scheme to determine phase shifts and polarization transport laws for bent SMF in flat space-time (neglecting bending losses), thus providing the first rigorous derivation of Rytov's law, which had already been verified experimentally [21, 22] but had previously been derived only using ray optics methods [23–25] or approximation schemes that neglected the internal structure of SMF [26–28].

The present paper combines and extends the methods of Refs. [20, 29, 30] to provide a comprehensive model of light-propagation in single-mode step-index fibers in general stationary space-times. The result of the calculation is a series of transport laws, formulated in equations (36a) to (36d), that describe the variation of the frequency, wavelength, phase, and polarization along a bent fiber, respectively.

The notation used in this paper is summarized in appendix A.

II. STATIONARY FIBERS

Single mode fibers (SMF) consist of an optically dense core within an optically less dense cladding. Whereas nanofibers consist of a glass core with ambient air acting as the cladding, the core and cladding of typical SMF are made of fused silica and are shielded by additional protective layers, see fig. 1. This section models such fibers in stationary curved space-times, thus providing a basis for the description of light propagation within such fibers.

Stationary space-times are described by a metric $g_{\mu\nu}$ that admits a timelike Killing vector field \mathcal{K}^μ [31, Chap. 18]. The dimensionless norm $\zeta = \sqrt{-g_{\mu\nu}\mathcal{K}^\mu\mathcal{K}^\nu}/c$ will henceforward be referred to as the lapse. Locally, there exist coordinates (t, x^i) with respect to which \mathcal{K}^μ takes the form $(\mathcal{K}^\mu) = (1, \mathbf{0})$. The one-form $\mathcal{K}_\mu \equiv g_{\mu\nu}\mathcal{K}^\nu$ can then be parametrized as $(\mathcal{K}_\mu) = c^2\zeta^2(-1, \xi_i/c)$, where ξ_i will be referred to as the

* thomas.mieling@univie.ac.at;

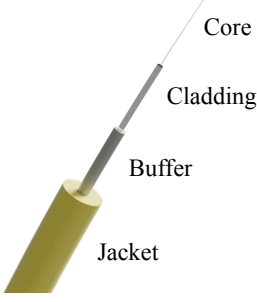


Figure 1. Schematic representation of the internal structure of single-mode step-index fibers. The electromagnetic modes are supported in the core (typical diameters $2a < 10 \mu\text{m}$) and decay at exponential rates in the cladding (diameters on the order of $100 \mu\text{m}$). For the purpose of solving Maxwell's equations, the protective layers (buffer and jacket with typical outer diameters on the order of 1 mm) are thus irrelevant.

shift.¹ Finally, defining the spatial metric $l_{\mu\nu}$ relative to \mathcal{K}^μ as $l_{\mu\nu} = g_{\mu\nu} + \mathcal{K}_\mu \mathcal{K}_\nu / (c\zeta)^2$ yields the decomposition [32, Sect. 9.6]

$$g = -\zeta^2 (cdt - \xi_i dx^i)^2 + l_{ij} dx^i dx^j. \quad (1)$$

Compared to the ADM metric $g_{ij}^{\text{ADM}} = l_{ij} - \zeta^2 \xi_i \xi_j$, which describes the geometry of the level-sets $t = \text{constant}$ [33], the spatial metric l_{ij} describes the geometry of events that are simultaneous relative to the four-velocity $u^\mu = \mathcal{K}^\mu / \zeta$ [34, § 84]. Moreover, the spatial metric l_{ij} as defined here is invariant under the gauge transformations described in footnote 1, whereas g_{ij}^{ADM} is not invariant under such transformations. Based on the above decomposition of the space-time metric, the shape of optical fibers “at rest” can be modeled in the spatial geometry that is described by the metric l_{ij} . To this end, it is beneficial to use spatial coordinates that are adapted to the fiber's baseline Γ . Denoting by $t^i = d\Gamma^i(s)/ds$ the unit tangent, where s is the arc length, the principal normal is $\nu^i = D_s t^i$ where D_i is the spatial Levi-Civita derivative. In regions of non-zero curvature $\kappa = (t^i \nu_i \nu_j)^{1/2}$, the unit normal is given by $n^i = \nu^i / \kappa$, and the unit binormal is $b^i = \epsilon^i_{jk} t^j n^k$, where ϵ_{ijk} is the spatial Levi-Civita (pseudo-)tensor. The frame (t^i, n^i, b^i) satisfies the Frenet–Serret equations [35, p. 34]

$$\mathcal{D}_s t^i = 0, \quad \mathcal{D}_s n^i = +\tau b^i, \quad \mathcal{D}_s b^i = -\tau n^i, \quad (2)$$

where $\tau = +b_i D_s n^i = -n_i D_s b^i$ is the torsion of Γ , and \mathcal{D}_s denotes the Fermi–Walker derivative

$$\begin{aligned} \mathcal{D}_s w^i &= D_s w^i + t^i \nu_k w^k - \nu^i t_k w^k \\ &\equiv D_s w^i - \kappa \epsilon^i_{jk} b^j w^k. \end{aligned} \quad (3)$$

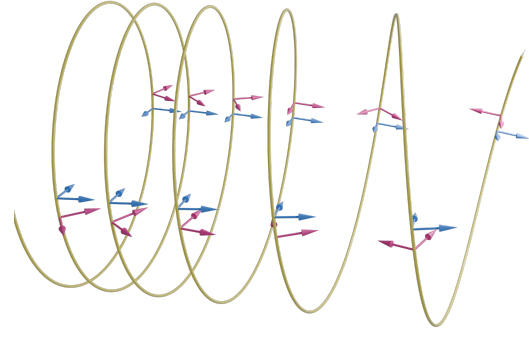


Figure 2. Schematic representation of a coiled optical fiber together with the Frenet–Serret frame (blue) and the Bishop frame (magenta). Whereas the Frenet–Serret frame is obtained by differentiating the curve's unit tangent, the Bishop frame is obtained by Fermi–Walker transport. Equation (2) implies that the angle between the two frames increases with arc length at a rate that is equal to the curve's torsion.

References [26–28] described light propagation in optical fibers using the Frenet–Serret basis. However, since this frame is undefined at points of vanishing curvature the following analysis uses, instead, an orthonormal frame (t^i, f_1^i, f_2^i) satisfying Bishop's equations [36]

$$\mathcal{D}_s f_1^i = 0, \quad \mathcal{D}_s f_2^i = 0. \quad (4)$$

Figure 2 provides a graphical illustration of the transverse Frenet–Serret frame (n^i, b^i) and the Fermi–Walker-transported Bishop frame (f_1^i, f_2^i) for a coiled fiber. The latter frame can be used to erect spatial Fermi coordinates $(s, x^1, x^2) \equiv (s, x^\alpha)$, see, e.g., Ref. [20, Appendix A]. In these coordinates, the physical distance of a point (s, x^α) from the baseline is given by $\sqrt{\delta_{\alpha\beta} x^\alpha x^\beta}$, so circles and cylinders around the baseline are accurately represented. Moreover, the series-expansion of the spatial metric around the baseline reads

$$\begin{aligned} l &= [(1 - \nu_\alpha x^\alpha)^2 - R_{s\alpha s\beta} x^\alpha x^\beta] ds^2 \\ &+ \frac{4}{3} R_{s\alpha\beta\gamma} x^\alpha x^\beta ds dx^\gamma \\ &+ [\delta_{\alpha\beta} - \frac{1}{3} R_{\alpha\gamma\beta\delta} x^\gamma x^\delta] dx^\alpha dx^\beta \\ &+ O[(\delta_{\alpha\beta} x^\alpha x^\beta)^{3/2}], \end{aligned} \quad (5)$$

where all components of the spatial Riemann tensor R_{ijkl} are evaluated on the baseline Γ . The deviations from the canonical form of the metric arising here have the same structure as in the Lorentzian case [37, 38]. Similarly to the spatial metric l_{ij} , the lapse can be expanded as a Taylor series in the form

$$\begin{aligned} \zeta(s, x^\alpha) &= \zeta(s) + \zeta_{,\alpha}(s) x^\alpha \\ &+ \frac{1}{2} \zeta_{,\alpha\beta}(s) x^\alpha x^\beta + O[(\delta_{\alpha\beta} x^\alpha x^\beta)^{3/2}], \end{aligned} \quad (6)$$

and analogous equations apply to the components ξ_i of the shift.² These series expansions provide a good approximation

¹ Apart from allowing arbitrary t -independent transformations of the spatial coordinates x^i , the setup also allows for a certain “gauge freedom” that arises from the possibility of redefining the temporal coordinate as $t' = t + \theta$ provided that θ is any smooth function of the spatial coordinates x^i . This induces a “gauge transformation” of the shift of the form $\xi'_i = \xi_i + c \partial_i \theta$.

² One generally has $\zeta_{,\alpha} \equiv \partial_\alpha \zeta = D_\alpha \zeta$, but in the considered coordinates it also holds that $\zeta_{,\alpha\beta} \equiv \partial_\alpha \partial_\beta \zeta = D_\alpha D_\beta \zeta$ and $\xi_{\alpha,\beta} \equiv \partial_\beta \xi_\alpha = D_\beta \xi_\alpha$. This is because (up to symmetry) the only non-trivial spatial Christoffel symbols along the baseline Γ are $\Gamma_{\alpha s s} = +\nu_\alpha$ and $\Gamma_{s s \alpha} = -\nu_\alpha$.

to $g_{\mu\nu}$ within the optical fiber whenever the characteristic length scales of the space-time geometry are significantly larger than the fiber's diameter. In practice, this is always satisfied.

Due to the accurate representation of cylinders by Fermi coordinates, step-index fibers can be described as in Euclidean space. In particular, for fibers with translation-invariant and circularly symmetric cross-sections, the fiber core corresponds to a disk in the (x^1, x^2) -plane, and the additional layers (cladding, buffer, and jacket) form concentric annuli.

To describe light propagation in SMF, one must describe not only the geometry of its internal structure but also its electromagnetic properties. As is common practice, the following calculations model such fibers as linear, isotropic and non-magnetic dielectrics with constant real refractive indices n_i in each layer [1, Sect. 2.4.3]. Additionally, due to the rapid radial decay of the electromagnetic field in the cladding, its outer radius is set to infinity in the following calculations [39, Sect. 3.1]. Under these assumptions, the constitutive equation relating the electromagnetic field-strength $F_{\mu\nu}$ (a two-form) to the excitation $\mathfrak{G}^{\mu\nu}$ (a bivector-density) can be written as $\mathfrak{G}^{\mu\nu} = \frac{1}{2}\mathfrak{X}^{\mu\nu\rho\sigma}F_{\rho\sigma}$ [40, Sect. VI.2], in which the constitutive tensor density $\mathfrak{X}^{\mu\nu\rho\sigma}$ can be expressed in terms of Gordon's contravariant optical metric $\tilde{g}^{\mu\nu} = l^{\mu\nu} - (n^2/c^2)u^\mu u^\nu$ as [41]

$$\mathfrak{X}^{\mu\nu\rho\sigma} = \sqrt{-g}[\tilde{g}^{\mu\rho}\tilde{g}^{\nu\sigma} - \tilde{g}^{\mu\sigma}\tilde{g}^{\nu\rho}]. \quad (7)$$

In the following, electromagnetic modes are computed in terms of the four-potential A_μ . Since Maxwell's equations do not directly lead to well-posed evolution equations for A_μ , the approach taken here is to work, instead, with the field equation of Ref. [17], namely

$$\nabla_\mu G^{\mu\nu} + \tilde{g}^{\mu\nu}\nabla_\mu\chi = 0, \quad (8)$$

where $G^{\mu\nu} = \tilde{g}^{\mu\rho}\tilde{g}^{\nu\sigma}(dA)_{\rho\sigma}$ and $\chi = \nabla_\mu(\tilde{g}^{\mu\nu}A_\nu)$. Contrary to Maxwell's equations, eq. (8) constitutes a well-posed evolution equation for the potential, and if A_μ is a solution to eq. (8) with $\chi = 0$, then $F_{\mu\nu} = (dA)_{\mu\nu}$ and $\mathfrak{G}^{\mu\nu} = \sqrt{-g}G^{\mu\nu}$ satisfy Maxwell's equations, together with the constitutive equation, in the form

$$(dF)_{\mu\nu\rho} = 0, \quad (\text{div } \mathfrak{G})^\mu = 0, \quad \mathfrak{G}^{\mu\nu} = \frac{1}{2}\mathfrak{X}^{\mu\nu\rho\sigma}F_{\rho\sigma}. \quad (9)$$

This procedure is analogous to the method of solving the "relaxed Einstein equations" described in Ref. [42, Sect. 6.2].

In the present case, obtaining exact closed-form solutions to eq. (8) is infeasible. The following analysis is thus based on a perturbative expansion in a parameter $\varepsilon \ll 1$ that derives from the assumption that certain geometric quantities are small and gradually varying when compared to a typical length scale ℓ_0 associated to electromagnetic radiation in SMF (such as the fiber's core radius ϱ or the vacuum wavelength $2\pi c/\omega$). Specifically, a dimensionless function φ along the fiber's baseline Γ will be said to be k -gradual if it can be written in the form $\varphi(s) = \varepsilon^k \hat{\varphi}(\varepsilon s/\ell_0)$, where $\hat{\varphi}$ is a bounded function all of whose derivatives do not exceed the order of magnitude of $\hat{\varphi}$ itself. The following analysis assumes ζ to be 0-gradual, that $\ell_0\zeta_{,i}$, ξ_i , $\ell_0\nu_i$, are 1-gradual, and $\ell_0^2\zeta_{,ij}$, $\ell_0\xi_{i,j}$, $\ell_0^2R_{ijkl}$ are assumed

to be 2-gradual.³ More explicitly, these assumptions require the existence of a parameter $\varepsilon \ll 1$ such that

$$\varrho\omega/c = O(1), \quad \zeta = O(1), \quad (10a)$$

$$\xi_i = O(\varepsilon), \quad \varrho\nu_i = O(\varepsilon), \quad (10b)$$

$$\varrho^2R_{ijkl} = O(\varepsilon^2), \quad \varrho D_i f = f O(\varepsilon), \quad (10c)$$

where, in the last expression, f ranges over the functions ζ , ξ_i , R_{ijkl} and their derivatives, all of which are gradually varying in the sense of depending on the arc length s solely through $\varepsilon s/\ell_0$. Equation (10a) expresses that the optical wavelength is on the order of the fiber core radius and that the lapse function can be of order unity (it is equal to 1 for inertial coordinates in flat space-time). Further, eq. (10b) requires the rotation rate of the fiber to be small (bounding the shift ξ_i) and the fiber bending radius to be large compared to the core radius (bounding $\varrho\nu_i$ and hence also $\varrho\kappa$). Finally, eq. (10c) requires the spatial curvatures to be one order smaller than the previously considered quantities (so that R_{ijkl} is at most on the order of $\nu_i\nu_j$), and that taking transverse derivatives of the discussed quantities increases the order in ε by one. These assumptions generalize the weak-bending assumption formulated in Ref. [20] and are analogous to the scaling hypotheses underlying models of the gravitational and electromagnetic self-forces [43, 44]. While the smallness assumptions in eq. (10) are satisfied in typical SMF, they can be violated in tightly bent nanofibers [45] and would, in principle, also fail for relativistic rotational velocities or strong tidal forces with curvature radii below a micrometer (though such violations do not occur in practical applications).

III. PERTURBATIVE SCHEME

To solve, perturbatively, for the electromagnetic modes in the setup described above, it is useful to introduce dimensionless cylindrical coordinates $(x^0, \sigma, r, \vartheta)$ via

$$t = \ell_0 x^0/c, \quad x^1 = \ell_0 r \cos \vartheta, \quad (11a)$$

$$s = \ell_0 \sigma, \quad x^2 = \ell_0 r \sin \vartheta, \quad (11b)$$

where ℓ_0 is the optical length scale introduced in the previous section. For definiteness, for SMF with translation-invariant circular cross-sections, maximal simplification of the equations is achieved by setting ℓ_0 to the core radius ϱ (on the order of micrometers). Moreover, since the calculation makes use of Fourier series in ϑ , it is advantageous to define the complex frame

$$f_\pm^i = \frac{1}{\sqrt{2}}(f_1^i \mp i f_2^i), \quad (12)$$

³ The underlying heuristic behind these assumptions is that the fiber's curvature and the ambient geometry have characteristic length scales ℓ that far exceed the optical length scale ℓ_0 . All functions listed above, except for ξ_i are thus naturally of the form described above with ε replaced by $\varepsilon' = \ell_0/\ell \ll 1$. For technical reasons, the following analysis also requires the (dimensionless) shift ξ_i to be small. Assuming a uniform bound $|\xi_i| < \varepsilon'' \ll 1$, these assumptions can be cast into the form given above by setting $\varepsilon = \max\{\varepsilon', \varepsilon''\}$.

with the normalization chosen such that $l_{ij} f_+^i f_-^j = 1$, since the number of + and - subscripts in a term determines its ‘‘Fourier index,’’ i.e., the integer m in the expression $e^{im\theta}$. For example, setting $v_\pm = v_i f_\pm^i$, one has $v_\alpha x^\alpha / \ell_0 = (r/\sqrt{2})(v_+ e^{+i\theta} + v_- e^{-i\theta})$.

Although it is common practice to study Maxwell’s equations in optical fibers using the coordinate coframe dx^μ associated to cylindrical coordinates [8, 39], the approach taken here is to use, instead, the complex coframe

$$e^0 = \zeta(s)[dx^0 - \xi_\sigma d\sigma], \quad e^\sharp = \frac{1}{\sqrt{2}}(dr - ir d\theta), \quad (13a)$$

$$e^\parallel = d\sigma, \quad e^\flat = \frac{1}{\sqrt{2}}(dr + ir d\theta), \quad (13b)$$

since this leads to fully decoupled field equations at leading order, cf. Refs. [17, 20, 46].⁴ Monochromatic modes, i.e., traveling waves with constant Killing frequency ω_* , can be computed perturbatively using the ansatz $A_\mu = A_b e^{i\psi}$ with

$$A_b = a_b(r, \theta, \varsigma) e^{i\psi}, \quad (14)$$

where ψ is the phase function

$$\psi = -\omega_* \left[t - \xi_\alpha(s) x^\alpha / c - \int \xi_s(s) \frac{ds}{c} \right] \pm \int \beta(s) ds, \quad (15)$$

with the local propagation parameter $\beta > 0$ (such that the sign determines the direction of light propagation) and the amplitudes a_b being expanded as

$$\beta = \sum_{j \in \mathbb{N}} \varepsilon^j \beta^{(j)}(\varsigma), \quad (16)$$

$$a_b = \sum_{j \in \mathbb{N}} \sum_{m \in \mathbb{Z}} \varepsilon^j e^{im\theta} a_b^{(j,m)}(r, \varsigma). \quad (17)$$

In these and the following equations, σ and $\varsigma = \varepsilon\sigma$ are treated as ‘‘independent variables’’ in the sense of the multiple-scales method [47, Chap. 11]. The explicit form of the phase function ψ can be motivated using geometrical optics: interpreting $k_\mu = (d\psi)_\mu$ as the local wave-covector along the baseline, one has $k_\mu = -(\omega/c^2)u_\mu \pm \beta(ds)_\mu$, where $\omega = \omega_*/\zeta$ is the frequency relative to the medium. The quantity $n_{\text{ph}} = c\beta/\omega$ can thus be interpreted as the mode’s phase index that must be determined from the field equations (it typically lies between the core index n_1 and the cladding index n_2). In the following, the leading-order contribution $\bar{n} = c\beta^{(0)}/\omega$ will be referred to as the effective index.⁵ Independent of heuristics based on geometrical optics, the given ansatz for ψ yields a particularly simple form of the perturbative equations satisfied by a_b . In

particular, matching terms of equal order in ε and equal Fourier index, the equations reduce to a recursive system of the form

$$\mathbf{H}^{(m)} a^{(j,m)} = \Sigma_{\text{bulk}}^{(j,m)}, \quad \mathbf{A}^{(m)} a^{(j,m)} = \Sigma_{\text{intf.}}^{(j,m)}, \quad (18)$$

where $\mathbf{H}^{(m)}$ is a Helmholtz operator and $\mathbf{A}^{(m)}$ is an operator encoding the discontinuities of the fields at the core-cladding interface, see appendices B and C for explicit expressions.

A. Homogeneous Equations

To understand the structure of the problem, it is instructive to consider, first, the homogeneous problem

$$\mathbf{H}^{(m)} a = 0, \quad \mathbf{A}^{(m)} a = 0. \quad (19)$$

The general solution to $\mathbf{H}^{(m)} a = 0$ that is regular on the baseline and decays exponentially in the cladding is given by

$$f^{(m)}[\mathbf{q}] = (f_m(q_0), f_m(q_\parallel), f_{m+1}(q_\sharp), f_{m-1}(q_b)), \quad (20)$$

where $\mathbf{q}_b = (q_b^{\text{core}}, q_b^{\text{clad.}})$ are coefficients that may depend on ς , and f_m is given explicitly in terms of Bessel functions:

$$f_m(q^{\text{core}}, q^{\text{clad.}}) = \begin{cases} q^{\text{core}} J_m(ur)/J_m(u) & \text{in the core,} \\ q^{\text{clad.}} K_m(wr)/K_m(w) & \text{in the cladding.} \end{cases} \quad (21)$$

Here, the dimensionless coefficients u and w are given by

$$u = (\ell_0 \omega / c) \sqrt{n_1^2 - \bar{n}^2}, \quad w = (\ell_0 \omega / c) \sqrt{\bar{n}^2 - n_2^2}. \quad (22)$$

The interface condition $\mathbf{A}^{(m)} a = 0$ then takes the form

$$\mathbf{A}^{(m)} f^{(m)}[\mathbf{q}] \equiv \mathbf{M}^{(m)} \cdot \mathbf{q} = 0, \quad (23)$$

where $\mathbf{M}^{(m)}$ is a complex 8×8 matrix, see eq. (C2) for an explicit formula. Non-trivial solutions to eq. (19) exist if and only if $\mathbf{M}^{(m)}$ is singular, i.e., $\det \mathbf{M}^{(m)} = 0$. As shown in appendix C, the determinant factorizes as

$$\det \mathbf{M}^{(m)} \propto \mathcal{D}_{\text{ph},m} \mathcal{D}_{\text{g},m}^2, \quad (24)$$

where roots of $\mathcal{D}_{\text{ph},m}$ give rise to physical modes (satisfying $\chi = 0$ and $F_{\mu\nu} \neq 0$), whereas $\mathcal{D}_{\text{g},m} = 0$ yields so-called gauge modes ($F_{\mu\nu} = 0$) and ghost modes ($\chi \neq 0$) that are irrelevant for the present consideration [17, 29]. The function $\mathcal{D}_{\text{ph},m}$ has the structure $\mathcal{D}_{\text{ph}}(|m|, v, \bar{n}, n_1, n_2, \varrho/\ell_0)$, where v is the normalized frequency $v = (\ell_0 \omega / c) \sqrt{n_1^2 - \bar{n}^2}$. In a given fiber, non-trivial physical solutions to the homogeneous problem (19) exist if and only if \bar{n} is a root of $\mathcal{D}_{\text{ph},m}$ along the entire baseline, which entails the functional dependence $\bar{n} = \bar{n}(|m|, \omega)$. Note that \bar{n} generally varies along the fiber due to its dependence on $\omega = \omega_*/\zeta(s)$, but there is no explicit arc-length dependence of \bar{n} .

⁴ The complex frame (12) and the complex coframe (13) are complementary in the sense that f_+^i and f_-^i are defined along the baseline Γ ($r = 0$), whereas e_+^i and e_-^i are defined away from Γ ($r > 0$).

⁵ The analysis below shows that the relation between \bar{n} and ω , as defined here, is independent of the gravitational field. Such notation and nomenclature thus facilitates comparison with established literature on fiber optics.

If $\mathcal{D}_{\text{ph},m} = 0$, the matrix $\mathbf{M}^{(m)}$ has a one-dimensional kernel and co-kernel, so there is an eight-component column vector $\hat{\mathbf{q}}^m$ and an eight-component row vector $\hat{\mathbf{k}}^m$ satisfying

$$\mathbf{M}^{(m)} \cdot \hat{\mathbf{q}}^m = 0, \quad \hat{\mathbf{k}}^m \cdot \mathbf{M}^{(m)} = 0, \quad (25)$$

respectively, and every other solution \mathbf{q}^m (or \mathbf{k}^m) to such an equation is a multiple of the reference solution $\hat{\mathbf{q}}^m$ (or $\hat{\mathbf{k}}^m$), where the coefficient of proportionality may depend on ς .

B. Inhomogeneous Equations

Whereas the leading-order terms in eq. (17) satisfy homogeneous equations as given in eq. (19), higher-order terms satisfy inhomogeneous equations of the form

$$\mathbf{H}^{(m)} a = \Sigma_{\text{bulk}}, \quad \mathbf{A}^{(m)} a = \Sigma_{\text{intf}}. \quad (26)$$

The general solution to the inhomogeneous Helmholtz equation is given by

$$a = f^{(m)}[\mathbf{q}] + \mathbf{G}^{(m)} \Sigma_{\text{bulk}}, \quad (27)$$

where $f^{(m)}[\mathbf{q}]$ is defined in eq. (20) and $\mathbf{G}^{(m)}$ is the Green operator defined in appendix B. The interface condition in eq. (26) then takes the form

$$\mathbf{M}^{(m)} \cdot \mathbf{q} + \mathbf{A}^{(m)} \mathbf{G}^{(m)} \Sigma_{\text{bulk}} = \Sigma_{\text{intf}}, \quad (28)$$

where $\mathbf{M}^{(m)}$ is the same matrix as in eq. (23). Now, if $\mathbf{M}^{(m)}$ is non-singular, this equation admits a unique solution for \mathbf{q} . This non-resonant case occurs whenever the homogeneous problem only admits trivial solutions. If, alternatively, $\mathbf{M}^{(m)}$ is singular (resonant case), a necessary and sufficient condition for solvability of this equation is

$$\hat{\mathbf{k}}^m \cdot \mathbf{A}^{(m)} (\mathbf{G}^{(m)} \Sigma_{\text{bulk}} - \Sigma_{\text{intf}}) = 0, \quad (29)$$

where $\hat{\mathbf{k}}^m$ spans the co-kernel of $\mathbf{M}^{(m)}$, see eq. (25). If eq. (29) is satisfied, eq. (28) determines the coefficients \mathbf{q} up to a homogeneous solution that is proportional to $\hat{\mathbf{q}}^m$.

C. Perturbative Equations

Having established the main facts about the homogeneous equation (19) and the inhomogeneous equation (26), the system (18) can be solved iteratively. Specifically, separating the leading-order equations from the higher-order ones, one obtains

$$\mathbf{H}^{(m)} a^{(0,m)} = 0, \quad \mathbf{A}^{(m)} a^{(0,m)} = 0, \quad (30a)$$

$$\mathbf{H}^{(m)} a^{(j,m)} = \Sigma_{\text{bulk}}^{(j,m)}, \quad \mathbf{A}^{(m)} a^{(j,m)} = \Sigma_{\text{intf}}^{(j,m)}, \quad (30b)$$

with $m \in \mathbf{Z}$ and $j \geq 1$, where $\Sigma_{\text{bulk}}^{(j,m)}$ and $\Sigma_{\text{intf}}^{(j,m)}$ depend on the fields $a^{(j',m')}$ of order $j' < j$.

As demonstrated in section III A, for each $m \in \mathbf{Z}$, the system (30a) admits a non-trivial physical solution if and only if

$\mathcal{D}_{\text{ph},m} = 0$, which is an equation involving $\bar{n}(\varsigma)$, n_1 , n_2 , $\omega(\varsigma)$, and the core radius ϱ . These equations for different values of $|m|$ are mutually exclusive and can thus be solved only for at most two values of m that differ in sign. The following analysis focuses on the single-mode regime for which one has $m = \pm 1$ (this case allows for a particularly simple description of the electromagnetic polarization). For these ‘‘on-shell’’ Fourier indices $m = \pm 1$, the fields $a^{(0,m)}$ are determined uniquely up to amplitude factors of the form $\mathcal{A}_{\pm}^{(0)}(\varsigma)$, whereas all ‘‘off-shell’’ Fourier indices $m \neq \pm 1$ do not contribute at leading order: $a^{(0,m)} = 0$.

At next order, $j = 1$, the analysis in section III B shows that the inhomogeneous equations with m on-shell can be solved if and only if

$$\hat{\mathbf{k}}^m \cdot \mathbf{A}^{(m)} (\mathbf{G}^{(m)} \Sigma_{\text{bulk}}^{(1,m)} - \Sigma_{\text{intf}}^{(1,m)}) = 0. \quad (31)$$

Since $\Sigma_{\text{bulk}}^{(1,m)}$ depends on $\partial_{\varsigma} a^{(0,m)}$, these constraints determine the variation of the amplitudes $\mathcal{A}_{\pm}^{(0)}$ along ς (explicit equations are presented below). Equation (30b) with m on-shell and $j = 1$ can then be solved for $a^{(1,\pm)}$ up to free amplitudes $\mathcal{A}_{\pm}^{(1)}(\varsigma)$ whereas the equations with m off-shell have unique solutions without such free amplitudes.

The scheme just described extends to all $j \geq 1$. At each order, the solvability conditions

$$\hat{\mathbf{k}}^m \cdot \mathbf{A}^{(m)} (\mathbf{G}^{(m)} \Sigma_{\text{bulk}}^{(j,m)} - \Sigma_{\text{intf}}^{(j,m)}) = 0 \quad (32)$$

with $m = \pm 1$ determine transport equations for the amplitudes $\mathcal{A}_{\pm}^{(j-1)}(\varsigma)$ that are not determined from the previous-order equations. With eq. (32) satisfied, eq. (30b) with m on-shell can be solved uniquely up to two amplitudes $\mathcal{A}_{\pm}^{(j)}(\varsigma)$ (to be determined at next order), and eq. (30b) with m off-shell can be solved uniquely without any free parameters.

The terms arising in the second-order expansion of the metric tensor that are given explicitly in section II determine the solvability conditions (32) for $j \in \{0, 1, 2\}$. As shown in appendix D, these equations can be cast in the form of transport equations for the phase perturbation $\delta\psi = \pm \int \delta\beta ds$, where $\delta\beta = \beta - \bar{n}\omega/c$ accounts for all perturbation terms in eq. (16) that contribute to the phase ψ in eq. (15), and the Jones vector J_{α} (a complex transverse unit vector describing the state of polarization) along the baseline Γ :

$$\hat{D}\delta\psi = \delta\beta + O(\varepsilon^3/\ell_0), \quad (33a)$$

$$\hat{D}J_{\alpha} = \varpi \Xi_{\alpha}^{\beta} J_{\beta} + i H_{\alpha}^{\beta} J_{\beta} + O(\varepsilon^3/\ell_0). \quad (33b)$$

Here, \hat{D} is the spatial covariant derivative $\hat{D} = \pm D_s$ with the sign depending on the direction of light propagation as in eq. (15). Explicitly, the perturbation of the propagation coefficient, $\delta\beta$, in eq. (33a) can be written as

$$\delta\beta = \gamma_1 l^{\alpha\beta} z_{\alpha} z_{\beta} + \gamma_2 (K + l^{\alpha\beta} \zeta_{,\alpha\beta} / \zeta) + \gamma_3 R_{ss} + \gamma_4 \partial_s \zeta / \zeta + \gamma_5 \partial_s \partial_s \zeta / \zeta, \quad (34)$$

where γ_j are dimensionful coupling coefficients (phase coupling moments), $K = R_{xyxy}$ is the sectional curvature of the

transverse plane, R_{ss} is the longitudinal projection of the spatial Ricci tensor R_{ij} , and the vector $z_\alpha = v_\alpha + \zeta_{,\alpha}/\zeta$ combines the effects of the principal normal v_α and logarithmic derivatives of the lapse function ζ in transverse directions. The dimensionless coefficient ϖ in eq. (33b) describes the coupling to the antisymmetric tensor $\Xi_{\alpha\beta} = \zeta(d\xi)_{\alpha\beta}$, and $H_{\alpha\beta}$ is a symmetric and trace-free tensor of the form

$$H_{\alpha\beta} = \eta_1(z_\alpha z_\beta - \frac{1}{2}l_{\alpha\beta}l^{\gamma\delta}z_\gamma z_\delta) + \eta_2(w_{\alpha\beta} - \frac{1}{2}l_{\alpha\beta}l^{\gamma\delta}w_{\gamma\delta}). \quad (35)$$

Similarly to the coefficients γ_J in eq. (34), η_K are dimensionful coupling coefficients (polarization coupling moments), and $w_{\alpha\beta} = \underline{W}_{\alpha s \beta s}$ is a projection of the space-time Weyl tensor $\underline{W}_{\mu\nu\rho\sigma}$.

The explicit form of these transport equations can be derived using computer algebra systems – a reference implementation written in *Wolfram Language* is available online [48]. The values of the coupling coefficients ϖ , γ_J , and η_K depend on the normalized frequency ν and must generally be determined by quadrature (see the next section for numerical results).

IV. RESULTS

The results derived above can be summarized as a series of transport equations of the physical frequency ω , effective index \bar{n} , phase ψ , and transverse Jones vector J^i along the direction of light propagation:

$$\hat{D}\omega = -\omega \hat{D} \ln \zeta, \quad (36a)$$

$$\hat{D}\bar{n} = -\omega \frac{d\bar{n}}{d\omega} \hat{D} \ln \zeta, \quad (36b)$$

$$\hat{D}\psi = +\omega \bar{n}/c \pm \omega \zeta \xi_s/c + \delta\beta + O(\varepsilon^3/\ell_0), \quad (36c)$$

$$\hat{D}J^i = \pm \kappa \epsilon^i_{jk} b^j J^k + \varpi \epsilon^i_{jk} \Gamma^j J^k + iH^i_k J^k + O(\varepsilon^3/\ell_0), \quad (36d)$$

where the upper and lower signs apply to light propagating in parallel or antiparallel to the orientation of the fiber's baseline Γ , respectively. In these equations, \hat{D} denotes the covariant derivative along the direction of light propagation, i.e., $\hat{D} = \pm t^i D_i$, where t^i denotes the unit tangent of Γ . The quantities κ and b^i denote, respectively, the associated curvature and unit binormal. Apart from the spatial geometry of the fiber, these equations also depend on the space-time geometry through the lapse ζ and the shift ξ_i (both evaluated on the baseline). The effective index \bar{n} depends on the frequency ω (as defined relative to the fiber's rest frame) according to a dispersion relation that takes the same form as for straight fibers in flat space-time (see Ref. [39, Sect. 3.1] for details). The term $\delta\beta$ in eq. (36c) constitutes a perturbation to the propagation parameter and is given explicitly in eq. (34). The first term in eq. (36d) accounts for the difference between parallel transport and Fermi–Walker transport, see eq. (3). The second term in eq. (36d) describes a rotation of the electromagnetic polarization about the vector

$$\Gamma^i = \frac{1}{2} t^i \epsilon^{jkl} t_j \Xi_{kl} \equiv \zeta t^i \epsilon^{jkl} t_j \partial_k \xi_l, \quad (37)$$

with a rotation rate that depends on the dimensionless coupling constant ϖ . Finally, the last term in eq. (36d) gives rise to additional polarization dynamics that are described by the Hermitian, transverse, and traceless tensor given in eq. (35).

Whereas the dimensionful phase and polarization moments depend strongly on the normalized frequency ν , see fig. 3, variations of the gyrotropy factor ϖ are much smaller. For example, in fibers with refractive indices $n_1 = 1.4712$ and $n_2 = 1.4659$ (as were considered in Ref. [16]) and normalized frequencies $\nu = (\varrho\omega/c)\sqrt{n_1^2 - n_2^2}$ in the range $1 < \nu < 3$, the coefficients γ_J and η_K vary over multiple orders of magnitude while numerical variations of $\varpi \approx 0.341$ are on the order of 0.2%. Hence, the gyrotropy factor ϖ for any given fiber can be considered as constant with negligible error.

The following paragraphs elaborate on details of the transport equations (36a) to (36d).

a. Optical Phase and Redshift The gravitational redshift along the fiber is described by eq. (36a), which has the exact solution $\omega(s)/\omega(0) = \zeta(0)/\zeta(s)$. Even in the absence of material dispersion, waveguide dispersion entails that the redshift induces a change in effective index \bar{n} along the fiber according to eq. (36b). According to eq. (36c), the integral $\int \bar{n}\omega ds/c$ then determines the leading-order contribution to the phase ψ . If the lapse ζ is constant along the fiber, this leading-order contribution reduces to the standard form $\bar{n}\omega s/c$, but more general cases do not admit closed-form solutions. Whereas previously published derivations of such effects in SMF were restricted to specially aligned fibers [16, 17], the present formulas are free of such restrictions and hold also for fiber spools as will be used in the forthcoming GRAVITES experiment [8, 9]. While the interplay between the redshift and dispersion is beyond the current experimental sensitivity of the Mach–Zehnder interferometers used [16, Sect. 4.7], dispersive effects give rise to alternative methods for measuring the gravitational redshift in fibers [49].

b. Sagnac Effect The second term in eq. (36c) accounts for phases that are induced by the shift ξ_i . As this term changes sign when reversing the direction of light propagation, it can be isolated by interfering two waves that propagate in opposite directions through a fiber loop to produce the phase shift $\Delta\psi = 2\omega_* \oint_\Gamma \xi_i dx^i/c$, where $\omega_* = \omega\zeta$ denotes the constant Killing frequency.⁶ The present derivation of the Sagnac phase provides a rigorous extension of standard geometric-optics derivations [10, 11] to fiber optics without assuming specific fiber alignment as was done in previous analyses [14, 15]. Apart from Sagnac effects arising in interferometers rotating relative to Earth and those arising from Earth's spin [4, 6, 7], the above derivation also applies to frame-dragging-induced Sagnac phases of the kind described in Ref. [50].

c. Higher-Order Phase Corrections The last term in eq. (36c), with $\delta\beta$ given explicitly in eq. (34), describes higher-order phase corrections. They depend on various components

⁶ Since the Sagnac phase depends on the shift ξ_i through the loop integral $\oint \xi_i dx^i$, it is invariant under the gauge transformations described in footnote 1. For an interpretation of the Sagnac phase in terms of the twist of the Killing vector field \mathcal{K}^μ , see Ref. [11].

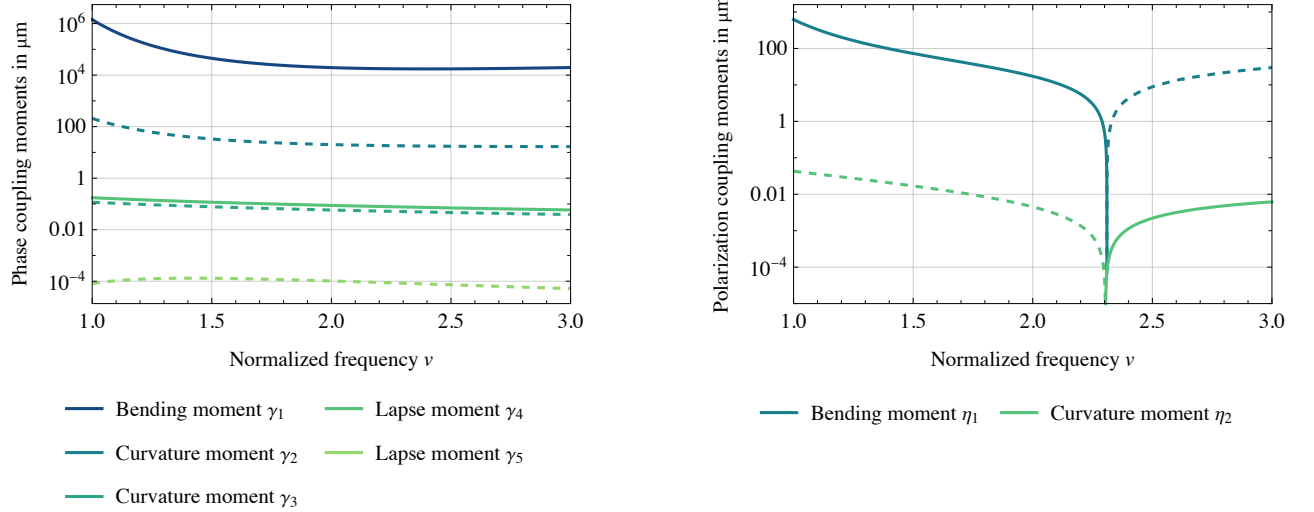


Figure 3. Dependence of the phase coupling moments γ_J (left) and polarization coupling moments η_K (right) on the normalized frequency $\nu = (\varrho\omega/c)\sqrt{n_1^2 - n_2^2}$, where ϱ is the fiber's core radius, ω is the optical frequency, and n_1 and n_2 are the refractive indices in the core and cladding, respectively. In these logarithmic plots, solid lines indicate positive values whereas dashed lines correspond to negative values. The values shown here were obtained for a single-mode fiber with core radius $\varrho = 4.1 \mu\text{m}$ and refractive indices $n_1 = 1.4712$ and $n_2 = 1.4659$.

of the space-time curvature tensor $R_{\mu\nu\rho\sigma}$ such as $R_{t\alpha t\beta} = \zeta D_\alpha D_\beta \zeta$ and $R_{s\alpha s\beta} = R_{s\alpha s\beta}$, where ζ is the lapse function and R_{ijkl} is the spatial curvature tensor. As can be seen in fig. 3, however, the dominant effect arises from the first term in eq. (34) that depends on the vector $z_\alpha = v_\alpha + D_\alpha \zeta / \zeta$. Since, the curvature of optical fiber spools [on the order of $1/(0.1 \text{ m})$] is significantly larger than the corresponding term arising from gravitational acceleration [$\text{g}/c^2 \approx 1/(9 \times 10^{15} \text{ m})$], bending effects as computed in Ref. [20] far exceed effects arising from non-trivial space-time geometry.

d. Rytov's Law The leading-order term in eq. (36d), $\pm \kappa \epsilon^i_{jk} b^j J^k$, ensures that J^i remains orthogonal to the direction of light propagation. If higher-order terms are negligible, the transport law for the polarization vector J_i reduces to Fermi–Walker transport, see eq. (3). At this level of approximation, J_i rotates relative to the transverse Frenet–Serret basis (n^i, b^i) according to $d\phi/ds = -\tau$, where τ is the torsion of the baseline, see eq. (2). This phenomenon is known as Rytov's law and has been demonstrated experimentally [21, 22]. Whereas previous derivations of this effect were restricted to flat space-time [20, 23, 24, 26–28], the analysis here shows how Rytov's law extends to curved space.

e. Geometrical Gyrotropy The second term in eq. (36d) describes an additional rotation in the transverse plane whose magnitude equals the norm of Γ^i , as defined in eq. (37), multiplied by the coupling constant ϖ . Such a polarization rotation was previously computed for light passing a rotating mass distribution using ray-optics approximations [51, 52]. This effect is commonly referred to as the gravitational Faraday effect owing to its mathematical analogy to the Faraday effect in media under the influence of external magnetic fields [53]. However, as the shift-induced rotation is reciprocal while the standard Faraday effect is non-reciprocal [54, Sect. 3.7.4],

such an effect can more accurately be regarded as a reciprocal gyrotropy effect that is analogous to optical activity in chiral materials. Since the present calculation is indifferent to the origin of ξ_i , it also applies to rotating systems in flat space-time. In particular, for an SMF with refractive indices as in fig. 3, the gyrotropy effect induced by a rotational frequency f causes a polarization rotation on the order of $(10^{-8} \text{ rad/m}) \cdot (f/\text{Hz})$.

f. Inverse Spin Hall Effects The tensor H_{ij} entering eq. (36d) describes inverse spin Hall effects. Whereas the ordinary spin Hall effect of light describes how the polarization affects the trajectories of light rays [55–57], in optical fibers the light trajectory is constrained and, instead, the polarization vector undergoes non-trivial dynamics, giving rise to an inverse spin Hall effect [20]. In the present case, eq. (35) shows that inverse spin Hall effects arise from fiber bending (described by the principal normal v_α), transverse gravitational acceleration (arising from logarithmic derivatives of the lapse function, $D_\alpha \zeta / \zeta$), and the space-time Weyl tensor $W_{\mu\nu\rho\sigma}$. The size of the respective coupling coefficients are plotted in fig. 3: similarly to the higher-order phase corrections, effects arising from gravitational acceleration and space-time curvature are multiple orders of magnitude smaller than those arising from fiber bending. Explicit expressions for such effects in helical fibers can be found in Ref. [20].

In conclusion, the transport equations (36a) to (36d) provide a generalization of multiple partial results that were derived previously. Specifically, prior models of the redshift and Sagnac effect in optical fibers were limited in admissible fiber geometries and considered these effects in isolation [15–19, 58]. The prior results on the redshift are obtained from eq. (36) by keeping only the ζ -terms (in particular, setting $\xi_i = 0$), and those on the Sagnac effect are reproduced by keeping only the ξ_i -terms (and setting $\zeta = 1$). Their unified description in general fiber geometries, however, constitutes a new result.

Similarly, by taking $\zeta = 1$, $\xi_i = 0$ and $R_{ijkl} = 0$, eq. (36d) reproduces the results of Ref. [20] that derived Rytov's law and inverse spin Hall effects for bent fibers in inertial systems. In this sense, the present model gives a unified description of bent fibers in non-inertial systems. Additionally, eq. (36) contains terms that depend on the space-time curvature tensor – these expressions thus cannot be reproduced by considering non-inertial motion in flat space-time. While some of these terms are analogous to expressions arising in curvature-couplings in free-space light propagation, their explicit form in fiber optics constitutes a new result of the perturbation theory developed here.

V. DISCUSSION

Generally speaking, gravitational effects on light propagation in media can be categorized into direct and indirect effects. Whereas direct effects arise from the dependence of Maxwell's equations on the space-time metric (more precisely, from the explicit dependence of the constitutive equation on $g_{\mu\nu}$), indirect effects arise from the medium's response to the gravitational field. The calculations provided here are restricted to direct effects as the cross-section of the fiber was assumed to be translation-invariant and the medium was modeled as linear, homogeneous, isotropic, and non-dispersive with constant refractive indices. The present analysis shows that the direct influence of gravity on light propagation in optical fibers is not limited to the gravitational redshift (previous calculations of which were restricted to specific fiber alignments and linearized gravity), but also includes higher-order phase perturbations and inverse spin Hall effects that depend on the curvature tensor of space-time.

Some indirect effects of gravity on light propagating in optical fibers have already been analyzed in the literature. Dispersion arising in modes of constant Killing frequency due to the gravitational redshift are described in Refs. [16, 49], geometric deformation effects and photoelastic effects in horizontally aligned fibers are modeled in Ref. [59], and similar photoelastic effects on solitons in vertically suspended fibers are analyzed in Refs. [18, 19]. The perturbative framework developed here could be used to extend these results to bent fibers and more general setups.

In addition to gravitational effects described above, the calculations presented here also account for a shift ξ_i that need not be of gravitational origin (shift vectors arise in rotating reference systems even if the ambient space-time is flat). While shift vectors are known to induce Sagnac phase shifts, explicit calculations of this effect were, so far, limited to ray-optics approximations or wave-optics calculations in specific fiber geometries. The present analysis provides a rigorous extension of these results to bent single-mode fibers without using ray approximations. Additionally, the calculation shows that light polarization undergoes a rotation whenever the shift vector has a non-zero curl. This geometrical gyrotropy effect is analogous to the gravitational Faraday effect.

Overall, the geometrical description of optical fibers developed here, specifically the use of the spatial metric l_{ij} in

eq. (1) rather than the ADM metric g_{ij}^{ADM} and the geometrically defined coordinate system based on Bishop's frame satisfying eq. (4), results in covariant transport laws (36a) to (36d) for the optical phase and polarization. This general scheme could be combined with numerical methods to describe light-propagation in optical fibers with other cross-sections (such as SMF that deviate from perfect translational symmetry along the axis or from rotational symmetry in the transverse planes, but also polarization-maintaining fibers or hollow-core fibers with more complex internal structures), as well as dispersive and non-linear media (as is relevant to the description of optical solitons).

ACKNOWLEDGMENTS

We are grateful to Marius Oancea and Piotr Chruściel for helpful discussions. Research by T.B.M. is funded by the European Union (ERC, GRAVITES, project no. 101071779). Views and opinions expressed are however those of the authors only and do not necessarily reflect those of the European Union or the European Research Council Executive Agency. Neither the European Union nor the granting authority can be held responsible for them. Research by M.H. was supported by an MSc Fellowship from the Vienna Doctoral School in Physics (VDSP).

Appendix A: Notation and Conventions

Throughout, this paper uses the Einstein summation convention for repeated indices (that applies whenever an index is printed once as a subscript and once as a superscript, but not to repeated subscripts or repeated superscripts). In these sums, the indices μ, ν, \dots range from 0 to 3; i, j, \dots from 1 to 3; α, β, \dots from 1 to 2; A, B, \dots range over the symbols + and –; and frame indices a, b, \dots range over the index set $\{0, \parallel, \#, b\}$.

The sign conventions used here are the same as in Ref. [60]. Specifically, the signature of the metric $g_{\mu\nu}$ is $(-, +, +, +)$, the Riemann tensor $\underline{R}^{\mu}{}_{\nu\rho\sigma}$ satisfies the Ricci identity in the form $\nabla_{\rho}\nabla_{\sigma}X^{\mu} - \nabla_{\sigma}\nabla_{\rho}X^{\mu} = \underline{R}^{\mu}{}_{\nu\rho\sigma}X^{\nu}$, and the Ricci tensor is defined as $\underline{R}_{\mu\nu} = \underline{R}^{\rho}{}_{\mu\rho\nu}$.

The exterior derivative of a differential form $\alpha_{\nu\rho\dots}$ is denoted by $(d\alpha)_{\mu\nu\rho\dots}$, and the divergence of a tensor density $\mathfrak{T}^{\mu\nu\rho\dots}$ is denoted by $(\text{div } \mathfrak{T})^{\nu\rho\dots}$. Symmetrization and anti-symmetrization of indices is indicated by parentheses and brackets, respectively.

Appendix B: Helmholtz Operators and Green Operators

The Helmholtz operator entering eq. (18) acts on a set of fields $a = (a_0, a_{\parallel}, a_{\#}, a_b)$ as

$$\mathbf{H}^{(m)} a = (H^{(m)} a_0, H^{(m)} a_{\parallel}, H^{(m+1)} a_{\#}, H^{(m-1)} a_b), \quad (\text{B1})$$

with

$$H^{(m)} = \frac{\partial^2}{\partial r^2} + \frac{1}{r} \frac{\partial}{\partial r} - \frac{m^2}{r^2} + (\ell_0^2 \omega^2 / c^2)(n^2 - \bar{n}^2). \quad (\text{B2})$$

Here, n is the local refractive index taking the constant values n_1 in the core, and n_2 in the cladding. This operator is known from the study of fiber optics in flat space-time [17, Sect. III.A.]

The associated Green operator $\mathbf{G}^{(m)}$ that is used in section III B is defined as

$$\mathbf{G}^{(m)} a = (G^{(m)} a_0, G^{(m)} a_{\parallel}, G^{(m+1)} a_{\#}, G^{(m-1)} a_b), \quad (\text{B3})$$

with

$$G^{(m)} f = \begin{cases} G_{\text{core}}^{(m)} f & \text{in the core,} \\ G_{\text{clad.}}^{(m)} f & \text{in the cladding,} \end{cases} \quad (\text{B4})$$

in which $G_{\text{core}}^{(m)}$ and $G_{\text{clad.}}^{(m)}$ are defined as

$$G_{\text{core}}^{(m)} f(r) = + \frac{\pi}{2} Y_m(ur) \int_0^r J_m(u\rho) f(\rho) \rho d\rho + \frac{\pi}{2} J_m(ur) \int_r^{r_*} Y_m(u\rho) f(\rho) \rho d\rho, \quad (\text{B5a})$$

$$G_{\text{clad.}}^{(m)} f(r) = - I_m(wr) \int_r^\infty K_m(w\rho) f(\rho) \rho d\rho - K_m(wr) \int_{r_*}^r I_m(w\rho) f(\rho) \rho d\rho. \quad (\text{B5b})$$

The free parameter r_* can be chosen arbitrarily to simplify explicit calculations by making the second terms in eqs. (B5a) and (B5b) vanish at any fixed radius. Independent of the choice of r_* , this operator satisfies $\mathbf{H}^{(m)} \mathbf{G}^{(m)} a = a$, as can be verified using the Wroński determinants

$$\begin{vmatrix} J_m(x) & Y_m(x) \\ J'_m(x) & Y'_m(x) \end{vmatrix} = \frac{2}{\pi x}, \quad \begin{vmatrix} K_m(x) & I_m(x) \\ K'_m(x) & I'_m(x) \end{vmatrix} = \frac{1}{x}, \quad (\text{B6})$$

see, e.g., eqs. (9.1.6) and (9.6.15) in Ref. [61].

Appendix C: Interface Conditions

The explicit form of the discontinuity operator $\mathcal{A}^{(m)}$ that arises in eq. (18) is given by

$$\mathcal{A}^{(m)} a = \begin{pmatrix} \llbracket a_0 \rrbracket \\ \llbracket a_{\parallel} \rrbracket \\ \llbracket a_{\#} \rrbracket \\ \llbracket a_b \rrbracket \\ \llbracket \partial_r a_{\parallel} \rrbracket \\ \llbracket C_{m+1}^- a_{\#} - C_{m-1}^+ a_b \rrbracket \\ \llbracket i n^2 \omega a_0 + C_{m+1}^- a_{\#} + C_{m-1}^+ a_b \rrbracket \\ \llbracket n^2 \{ \partial_r a_0 + \frac{i\omega}{\sqrt{2}} (a_{\#} + a_b) \} \rrbracket \end{pmatrix}, \quad (\text{C1})$$

where $\llbracket f \rrbracket = (f|_{r \downarrow (\varrho/\ell_0)}) - (f|_{r \uparrow (\varrho/\ell_0)})$ denotes the jump of a function at the core-cladding interface, and $C_m^\pm = \frac{1}{\sqrt{2}} (\partial_r \mp m/r)$.

The corresponding matrix $\mathbf{M}^{(m)}$ as defined in eq. (23) has the explicit form

$$\mathbf{M}^{(m)} = \begin{pmatrix} +1 & 0 & 0 & 0 & -1 & 0 & 0 & 0 \\ 0 & +1 & 0 & 0 & 0 & -1 & 0 & 0 \\ 0 & 0 & -u \mathcal{I}_m^+ & 0 & 0 & 0 & +w \mathcal{K}_m^+ & 0 \\ 0 & 0 & 0 & +u \mathcal{I}_m^- & 0 & 0 & 0 & +w \mathcal{K}_m^- \\ 0 & +u^2 \mathcal{I}_m & 0 & 0 & 0 & -w^2 \mathcal{K}_m & 0 & 0 \\ 0 & 0 & +u & +u & 0 & 0 & +w & -w \\ +i n_1^2 \omega & 0 & +\frac{u}{\sqrt{2}} & -\frac{u}{\sqrt{2}} & -i n_2^2 \omega & 0 & +\frac{w}{\sqrt{2}} & +\frac{w}{\sqrt{2}} \\ +n_1^2 u^2 \mathcal{I}_m & 0 & -\frac{i n_1^2 u \omega}{\sqrt{2}} \mathcal{I}_m^+ + \frac{i n_1^2 u \omega}{\sqrt{2}} \mathcal{I}_m^- & -n_2^2 w^2 \mathcal{K}_m & 0 & +\frac{i n_2^2 w \omega}{\sqrt{2}} \mathcal{K}_m^+ + \frac{i n_2^2 w \omega}{\sqrt{2}} \mathcal{K}_m^- \end{pmatrix}, \quad (\text{C2})$$

where the following abbreviations were used:

$$\mathcal{I}_m = \frac{J'_m(u)}{u J_m(u)}, \quad \mathcal{K}_m = \frac{K'_m(w)}{w K_m(w)}, \quad (\text{C3})$$

$$\mathcal{I}_m^\pm = \mathcal{I}_m \mp m/u^2, \quad \mathcal{K}_m^\pm = \mathcal{K}_m \mp m/w^2. \quad (\text{C4})$$

The parameters u and w arising here are defined in eq. (22). The determinant of the matrix $\mathbf{M}^{(m)}$ factorizes as

$$\det \mathbf{M}^{(m)} = \sqrt{2} u^2 w^2 \mathcal{D}_{g,m}^2 \mathcal{D}_{\text{ph},m} \quad (\text{C5})$$

Here, the factor whose vanishing indicates gauge and ghost

modes takes the form

$$\mathcal{D}_{g,m} = u^2 \mathcal{I}_m - w^2 \mathcal{K}_m, \quad (\text{C6})$$

and the factor whose roots correspond to physical modes can be written as

$$\mathcal{D}_{\text{ph},m} = (\mathcal{I}_m + \mathcal{K}_m)(n_1^2 \mathcal{I}_m + n_2^2 \mathcal{K}_m) - \bar{m}^2, \quad (\text{C7})$$

where $\bar{m} = m \bar{n} v^2 / (u^2 w^2)$. The expressions arising here are the same as for straight optical fibers in flat space-time [17].

Appendix D: Derivation of Transport Laws

Equation (25) allows for arbitrary rescaling of the vectors \hat{q}^\pm but the interpretation of the multiplying amplitudes $\mathcal{A}_\pm^{(j)}$ is significantly simplified if the vectors \hat{q}^\pm are normalized consistently. As shown in Ref. [17, eq. (69a)], these two vectors can be chosen such that one of them can be obtained from the other by a permutation of the components and some changes of sign. The specific details of such a normalization play no significant role however: both $(\hat{q}^+)_{\text{b}}^{\text{core}} = (\hat{q}^-)_{\text{#}}^{\text{core}} = 1$ (as is natural when taking the weak-guidance limit) and $(\hat{q}^\pm)_0^{\text{core}} = 1$ lead to the same numerical values in eqs. (33a) and (33b).

Assuming such a symmetric normalization of the vectors \hat{q}^\pm , the solvability conditions (32) for $j = 1$ and $j = 2$ can be written in the form

$$L \mathcal{A}_A^{(0)} = C_0 \mathcal{A}_A^{(0)}, \quad (\text{D1})$$

$$L \mathcal{A}_A^{(1)} = C_0 \mathcal{A}_A^{(1)} + C_A^B \mathcal{A}_B^{(0)}, \quad (\text{D2})$$

where $L = \frac{d}{d\zeta} \pm i\ell_0\beta^{(1)}$ is a differential operator involving the first-order term in the expansion (16), and C_0 is a coefficient depending on the specific normalization of \hat{q}^\pm (in both normalization schemes mentioned above, one has $C_0 = c_0(v)\dot{\zeta}'(\zeta)/\dot{\zeta}(\zeta)$ for some function c_0 that can be determined numerically). Using computer algebra systems – an implementation in *Wolfram Language* is available online [48] – one finds that the coupling coefficients C_A^B can be written as

$$C_A^B = \bar{C}_A^B \mp i(\ell_0\beta^{(2)})\delta_A^B + [c_1(v)\ell_0\beta^{(1)}\dot{\zeta}'/\dot{\zeta} + c_2(v)\ell_0\beta^{(1)}\dot{\zeta}''/\dot{\zeta}']\delta_A^B, \quad (\text{D3})$$

where \bar{C}_A^B has the following structure. Denoting by $l_{AB} = l_{ij}f_A^i f_B^j$ the components of the transverse metric in the complex frame $(f_A^i) = (f_+^i, f_-^i)$, the matrix $\bar{C}_{AB} = \bar{C}_A^D l_{DB}$ can be written as

$$\bar{C}_{AB} = \sum_{\tau} c_{AB}(v)\tau_{AB}(\zeta), \quad (\text{D4})$$

where τ ranges over all terms derived from the rescaled quantities $\dot{\zeta}, \dot{\zeta}_{,\alpha}, \dot{\zeta}_{,\alpha\beta}, \dot{\zeta}_{\alpha}, \dot{\zeta}_{\alpha,\beta}, \dot{\nu}_{\alpha}, \dot{R}_{\alpha\beta\gamma\delta}$ and $\dot{R}_{\alpha\sigma\beta\sigma}$ (as defined at the end of section II) that have the appropriate Fourier index. For example, the sum for C_{++} involves, i.a., the terms $(\dot{\nu}_+)^2, (\dot{\zeta}_+/\dot{\zeta})^2, \dot{\zeta}_{++}/\dot{\zeta}$, and $\dot{R}_{+\sigma+\sigma}$. The values of the coefficients c_{AB} must generally be computed using numerical integration.

Factorizing the amplitudes as $\mathcal{A}_A^{(j)} = \mathcal{A} J_A^{(j)}$ where the overall amplitude satisfies $d\mathcal{A}/d\zeta = C_0 \mathcal{A}$, one obtains

$$L J_A^{(0)} = 0, \quad L J_A^{(1)} = C_A^B J_B^{(0)}. \quad (\text{D5})$$

The amplitude \mathcal{A} exhibits a certain ‘‘gauge redundancy’’ that arises from the fact that the vectors q^\pm can be rescaled by any non-zero function λ as $q^\pm \rightarrow \lambda q^\pm$. Such a transformation is equivalent to a rescaling of the multiplying amplitude by $\mathcal{A} \rightarrow \lambda \mathcal{A}$, which induces the transformation $C_0 \rightarrow C_0 + \lambda^{-1} d\lambda/d\zeta$. Since eq. (D5) is unaffected by this ambiguity, the following analysis focuses on the quantities $J_A^{(0)}$ and $J_A^{(1)}$.

The transport equations (D5) can be combined by defining $J_A = J_A^{(0)} + \varepsilon J_A^{(1)} + O(\varepsilon^2)$, as can be motivated using renormalization methods described in Refs. [62, 63], to yield

$$L J_A = \varepsilon C_A^B J_B + O(\varepsilon^2). \quad (\text{D6})$$

As shown in Ref. [20], the two quantities J_+ and J_- can be identified with projections of a complex polarization vector J_i onto the frame f_\pm via $J_A = J_i f_A^i$. Now, the parameters $\beta^{(1)}$ and $\beta^{(2)}$ can be chosen arbitrarily without altering the physical content of the equations [this is because the splitting of the field in eq. (14) into amplitudes and a phase factor is not unique]. Particularly simple equations are obtained by setting $\beta^{(1)} = 0$ and choosing $\beta^{(2)}$ such that C_A^B becomes trace-free. This leads to the result

$$\begin{aligned} \ell_0\beta^{(2)} &= \tilde{\gamma}_1 \dot{R}_{+--+} + \tilde{\gamma}_2 \dot{R}_{\zeta\zeta} + \tilde{\gamma}_3 \dot{\zeta}_{,+} / \dot{\zeta} \\ &+ \tilde{\gamma}_4 \dot{\zeta}_{,\zeta} / \dot{\zeta} + \tilde{\gamma}_5 \dot{\zeta}_{,\zeta\zeta} / \dot{\zeta} + \tilde{\gamma}_6 \dot{\nu}_+ \dot{\nu}_- \\ &+ \tilde{\gamma}_7 \dot{\zeta}_{,+} \dot{\zeta}_{,-} / \dot{\zeta}^2 + \tilde{\gamma}_8 \dot{\nu}_{(+}\dot{\zeta}_{-)} / \dot{\zeta}, \\ C_{AB} &= \varpi(\dot{\zeta}_{A,B} - \dot{\zeta}_{B,A}) \\ &+ \tilde{\eta}_1(\dot{\nu}_A \dot{\nu}_B - l_{AB} \dot{\nu}_+ \dot{\nu}_-) \\ &+ \tilde{\eta}_2(\dot{\zeta}_{,A} \dot{\zeta}_{,B} - l_{AB} \dot{\zeta}_{,+} \dot{\zeta}_{,-}) / \dot{\zeta}^2 \\ &+ \tilde{\eta}_3(\dot{\nu}_{(A} \dot{\zeta}_{,B)} - l_{AB} \dot{\nu}_{(+}\dot{\zeta}_{-)} / \dot{\zeta} \\ &+ \tilde{\eta}_4(\dot{R}_{A\zeta B\zeta} - \frac{1}{2} l_{AB} \dot{R}_{\zeta\zeta}) \\ &+ \tilde{\eta}_5(\dot{\zeta}_{,AB} - l_{AB} \dot{\zeta}_{,+} / \dot{\zeta}. \end{aligned} \quad (\text{D7})$$

The dimensionless coefficients arising here [which generally depend on the normalized frequency ν and the sign in eq. (15)] can be determined by numerically implementing the scheme described in section III, in which the homogeneous solutions given in eq. (20) are evaluated on-shell by numerical root-finding of eq. (C7), and inserted into the source terms $\Sigma_{\text{bulk}}^{(j,m)}$ and $\Sigma_{\text{intf}}^{(j,m)}$ entering eq. (30b) that can be computed symbolically using computer algebra systems (the explicit expressions are extensive and not particularly illuminating).

Numerically, one finds that $\tilde{\gamma}_6 \approx \tilde{\gamma}_7 \approx \frac{1}{2} \tilde{\gamma}_8$ (to within 0.5 % relative error) and $\tilde{\eta}_1 \approx \tilde{\eta}_2 \approx \frac{1}{2} \tilde{\eta}_3$ (to within 1 % relative error) so that the contributions of the rescaled principal normal $\dot{\nu}_A$ and the rescaled logarithmic lapse derivative $\dot{\zeta}_{,A}/\dot{\zeta}$ can be expressed (to that level of accuracy) via a coupling to $\dot{\zeta}_A = \dot{\nu}_A + \dot{\zeta}_{,A}/\dot{\zeta}$. Similarly, one finds $\tilde{\eta}_4 \approx \tilde{\eta}_5$ (to within 3×10^{-5} absolute error; relative errors are undefined due to zeros of these coefficients) so that the terms involving the spatial Riemann tensor R_{ijkl} and second logarithmic lapse derivatives $\zeta_{,ij}/\zeta$ in eq. (D8) can be expressed in terms spatial components of the space-time Weyl tensor $\underline{W}_{\mu\nu\rho\sigma}$ since

$$\begin{aligned} \dot{W}_{A\zeta B\zeta} - \dot{l}_{AB} \dot{W}_{+\zeta-\zeta} &= \frac{1}{2}(\dot{R}_{A\zeta B\zeta} - \dot{l}_{AB} \dot{R}_{+\zeta-\zeta}) \\ &+ \frac{1}{2}(\dot{\zeta}_{,AB} - l_{AB} \dot{\zeta}_{,+} / \dot{\zeta}). \end{aligned} \quad (\text{D9})$$

Finally, the numerical analysis shows that $\tilde{\gamma}_1 \approx -\frac{1}{2} \tilde{\gamma}_2$ to within 0.4 % relative error.

The transport equations (33a) and (33b) are then obtained by transforming the rescaled quantities $\hat{\phi}$ entering eqs. (D7) and (D8) to their original form (as described at the end of section II) and using the fact that $\frac{d}{ds} = (\varepsilon/\ell_0) \frac{d}{d\zeta}$.

Some of the “numerical coincidences” described above can be explained by the conformal invariance of Maxwell’s equations. By rescaling the space-time metric by $(1 - x^\alpha \lambda_\alpha(s))^2$, where $\lambda_\alpha(s)$ are arbitrary functions, first-order terms in the expansion of the spatial metric component l_{ss} in eq. (5) and the lapse ζ in eq. (6) transform as $\nu_\alpha \rightarrow \nu_\alpha + \lambda_\alpha$ and $\zeta_{,\alpha} \rightarrow \zeta_{,\alpha} - \lambda_{\alpha}\zeta$. Choosing $\lambda_\alpha = \zeta_{,\alpha}/\zeta$ thus eliminates

first transverse derivatives of the lapse while simultaneously replacing $\nu_\alpha \rightarrow z_\alpha \equiv \nu_\alpha + \zeta_{,\alpha}/\zeta$ in the first-order expansion of the l_{ss} . Under such a conformal transformation, all second-order terms in eqs. (5) and (6) are also transformed, but as shown in fig. 3, their effects are multiple orders of magnitude smaller than those arising from the linear terms under consideration. The last numerical coincidence listed above, however, does not seem to arise from conformal invariance as the sectional curvature $K = R_{xyxy} = -R_{+--+}$ and second lapse derivatives do not directly combine to yield a component of the Weyl tensor.

-
- [1] J. M. Senior, *Optical Fiber Communications*, third ed. (Pearson Education, 2009).
- [2] B. Lee, Review of the present status of optical fiber sensors, *Optical Fiber Technology* **9**, 57 (2003).
- [3] C. Hilweg, D. Shadmany, P. Walther, N. Mavalvala, and V. Sudhir, Limits and prospects for long-baseline optical fiber interferometry, *Optica* **9**, 1238 (2022), arXiv:2208.09247 [physics.optics].
- [4] H. C. Lefèvre, The fiber-optic gyroscope: Challenges to become the ultimate rotation-sensing technology, *Optical Fiber Technology* **19**, 828 (2013).
- [5] M. Fink, F. Steinlechner, J. Handsteiner, J. P. Dowling, T. Scheidl, and R. Ursin, Entanglement-enhanced optical gyroscope, *New Journal of Physics* **21**, 053010 (2019), arXiv:1810.02213 [quant-ph].
- [6] M. Cromb, S. Restuccia, G. M. Gibson, M. Toroš, M. J. Padgett, and D. Faccio, Mechanical rotation modifies the manifestation of photon entanglement, *Physical Review Research* **5**, L022005 (2023).
- [7] R. Silvestri, H. Yu, T. Strömberg, C. Hilweg, R. W. Peterson, and P. Walther, Experimental observation of Earth’s rotation with quantum entanglement, *Science Advances* **10**, eado0215 (2024), arXiv:2310.16903 [quant-ph].
- [8] C. Hilweg, F. Massa, D. Martynov, N. Mavalvala, P. T. Chruściel, and P. Walther, Gravitationally induced phase shift on a single photon, *New Journal of Physics* **19**, 033028 (2017), arXiv:1612.03612 [quant-ph].
- [9] E. Polini, D. Macri, X. Yin, E. Oelker, P. Chruściel, G. Dvali, C. Hilweg, M. Hudelist, D. Lopez Mago, T. Mieling, T. Morling, M. Oancea, R. Silvestri, F. Steininger, H. Yu, P. Walther, and N. Mavalvala, Large-scale fiber interferometry to measure the gravitationally induced phase shift on entangled photons, in *Quantum 2.0 Conference and Exhibition* (Optica Publishing Group, 2024) p. QTh4C.3.
- [10] E. J. Post, Sagnac Effect, *Reviews of Modern Physics* **39**, 475 (1967).
- [11] A. Ashtekar and A. Magnon, The Sagnac effect in general relativity, *Journal of Mathematical Physics* **16**, 341 (1975).
- [12] M. Zych, F. Costa, I. Pikovski, T. C. Ralph, and Č. Brukner, General relativistic effects in quantum interference of photons, *Classical and Quantum Gravity* **29**, 224010 (2012), arXiv:1206.0965 [quant-ph].
- [13] T. B. Mieling, C. Hilweg, and P. Walther, Measuring space-time curvature using maximally path-entangled quantum states, *Phys. Rev. A* **106**, L031701 (2022), arXiv:2202.12562 [gr-qc].
- [14] H. C. Lefèvre and H. J. Arditty, Electromagnétisme des milieux diélectriques linéaires en rotation et application à la propagation d’ondes guidées, *Appl. Opt.* **21**, 1400 (1982).
- [15] T. B. Mieling, On the influence of Earth’s rotation on light propagation in waveguides, *Classical and Quantum Gravity* **37**, 225001 (2020), arXiv:1911.12156 [physics.optics].
- [16] R. Beig, P. T. Chruściel, C. Hilweg, P. Korrreich, and P. Walther, Weakly gravitating isotropic waveguides, *Classical and Quantum Gravity* **35**, 244001 (2018), arXiv:1807.04156 [gr-qc].
- [17] T. B. Mieling, Gupta-Bleuler quantization of optical fibers in weak gravitational fields, *Phys. Rev. A* **106**, 063511 (2022), arXiv:2207.13537 [quant-ph].
- [18] F. Spengler, A. Belenchia, D. Rätzel, and D. Braun, Optical solitons in curved spacetime, *Classical and Quantum Gravity* **40**, 145008 (2023), arXiv:2301.04986 [gr-qc].
- [19] A. Belenchia, F. Spengler, D. Rätzel, and D. Braun, Non-linear media in weakly curved spacetime: optical solitons and probe pulses for gravimetry, *New Journal of Physics* **26**, 083010 (2024), arXiv:2402.09930 [gr-qc].
- [20] T. B. Mieling and M. A. Oancea, Polarization transport in optical fibers beyond Rytov’s law, *Physical Review Research* **5**, 023140 (2023), arXiv:2302.10540 [physics.optics].
- [21] J. N. Ross, The rotation of the polarization in low birefringence monomode optical fibres due to geometric effects, *Optical and Quantum Electronics* **16**, 455 (1984).
- [22] A. Tomita and R. Y. Chiao, Observation of Berry’s topological phase by use of an optical fiber, *Phys. Rev. Lett.* **57**, 937 (1986).
- [23] E. Bortolotti, Sulle rappresentazioni conformi, e su di una interpretazione fisica del parallelismo di Levi-Civita, in *Atti della Reale Accademia Nazionale dei Lincei – Serie VI*, Rendiconti delle Sedute della Reale Accademia Nazionale dei Lincei – Classe di Scienze fisiche, matematiche e naturali, Vol. IV, edited by G. Bardi (Reale Accademia Nazionale dei Lincei, 1926) pp. 552–556.
- [24] Рытов, С. М., О Переходе От Волновой К Геометрической Оптике, Доклады Академии Наук СССР **18**, 263 (1938), English translation published in Ref. [25].
- [25] S. M. Rytov, Transition from wave to geometrical optics, in *Topological Phases in Quantum Theory*, edited by B. Markovski and S. I. Vinitzky (World Scientific Publishing, 1989) pp. 6–10.
- [26] M. V. Berry, Interpreting the anholonomy of coiled light, *Nature (London)* **326**, 277 (1987).
- [27] M.-Y. Lai, Y.-L. Wang, G.-H. Liang, F. Wang, and H.-S. Zong, Electromagnetic wave propagating along a space curve, *Phys. Rev. A* **97**, 033843 (2018), arXiv:1802.04059 [physics.optics].
- [28] M.-Y. Lai, Y.-L. Wang, G.-H. Liang, and H.-S. Zong, Geometrical phase and Hall effect associated with the transverse spin of light, *Phys. Rev. A* **100**, 033825 (2019).
- [29] T. B. Mieling, *Gupta–Bleuler quantization of the electromagnetic field in curved space-times with applications to gravitational photon interferometry*, *Doctoral thesis*, University of Vienna (2023).

- [30] M. Hudelist, *Space-time curvature-induced corrections to Rytov's law in optical fibers*, Master's thesis, University of Vienna (2024).
- [31] H. Stephani, D. Kramer, M. MacCallum, C. Hoenselaers, and E. Herlt, *Exact Solutions of Einstein's Field Equations*, second ed., Cambridge Monographs on Mathematical Physics (Cambridge University Press, 2003).
- [32] W. Rindler, *Relativity* (Oxford University Press, 2001).
- [33] R. Arnowitt, S. Deser, and C. W. Misner, Dynamical Structure and Definition of Energy in General Relativity, *Physical Review* **116**, 1322 (1959).
- [34] L. D. Landau and E. M. Lifshitz, *The Classical Theory of Fields*, fourth revised english ed., Course of Theoretical Physics, Vol. 2 (Pergamon Press, 1975) translated from the Russian by Morton Hamermesh.
- [35] M. Spivak, *A Comprehensive Introduction to Differential Geometry*, third ed., Vol. 2 (Publish or Perish, 1999).
- [36] R. L. Bishop, There is more than one way to frame a curve, *The American Mathematical Monthly* **82**, 246 (1975).
- [37] F. K. Manasse and C. W. Misner, Fermi Normal Coordinates and Some Basic Concepts in Differential Geometry, *Journal of Mathematical Physics* **4**, 735 (1963).
- [38] W.-T. Ni and M. Zimmermann, Inertial and gravitational effects in the proper reference frame of an accelerated, rotating observer, *Phys. Rev. D* **17**, 1473 (1978).
- [39] J.-M. Liu, *Photonic Devices* (Cambridge University Press, 2005).
- [40] E. J. Post, *Formal Structure of Electromagnetics* (North-Holland, 1962).
- [41] W. Gordon, Zur Lichtfortpflanzung nach der Relativitätstheorie, *Annalen der Physik* **377**, 421 (1923).
- [42] E. Poisson and C. M. Will, *Gravity* (Cambridge University Press, 2014).
- [43] S. E. Gralla and R. M. Wald, A rigorous derivation of gravitational self-force, *Classical and Quantum Gravity* **25**, 205009 (2008), arXiv:0806.3293 [gr-qc].
- [44] S. E. Gralla, A. I. Harte, and R. M. Wald, Rigorous derivation of electromagnetic self-force, *Phys. Rev. D* **80**, 024031 (2009), arXiv:0905.2391 [gr-qc].
- [45] L. Tong, R. R. Gattass, J. B. Ashcom, S. He, J. Lou, M. Shen, I. Maxwell, and E. Mazur, Subwavelength-diameter silica wires for low-loss optical wave guiding, *Nature (London)* **426**, 816 (2003).
- [46] F. Steininger, Proca Fields in Step-index Optical Fibres, arXiv:2302.12729 [physics.class-ph] (2023), preprint.
- [47] C. M. Bender and S. A. Orszag, *Advanced mathematical methods for scientists and engineers*, International Series in Pure and Applied Mathematics (McGraw-Hill, 1978).
- [48] T. B. Mieling, Source code for 'Fiber Optics in Curved Space-Times' (2024).
- [49] S. Manly and E. Page, Experimental feasibility of measuring the gravitational redshift of light using dispersion in optical fibers, *Phys. Rev. D* **63**, 062003 (2001), arXiv:gr-qc/0008004.
- [50] S. P. Kish and T. C. Ralph, Quantum effects in rotating reference frames, *AVS Quantum Science* **4**, 011401 (2022), arXiv:2202.05381 [quant-ph].
- [51] Скроцкий, Г. В., О влиянии силы тяжести на распространение света, Доклады Академии Наук СССР **114**, 73 (1957).
- [52] J. Plebanski, Electromagnetic Waves in Gravitational Fields, *Physical Review* **118**, 1396 (1960).
- [53] M. Nouri-Zonoz, Gravitoelectromagnetic approach to the gravitational Faraday rotation in stationary spacetimes, *Phys. Rev. D* **60**, 024013 (1999), arXiv:gr-qc/9901011 [gr-qc].
- [54] J. N. Damask, *Polarization Optics in Telecommunications*, Springer Series in Optical Sciences No. 101 (Springer Science+Business Media, 2004).
- [55] O. Hosten and P. Kwiat, Observation of the Spin Hall Effect of Light via Weak Measurements, *Science* **319**, 787 (2008).
- [56] K. Y. Bliokh, A. Niv, V. Kleiner, and E. Hasman, Geometrodynamics of spinning light, *Nature Photonics* **2**, 748 (2008), arXiv:0810.2136 [physics.optics].
- [57] M. A. Oancea, J. Joudioux, I. Y. Dodin, D. E. Ruiz, C. F. Paganini, and L. Andersson, Gravitational spin Hall effect of light, *Phys. Rev. D* **102**, 024075 (2020), arXiv:2003.04553 [gr-qc].
- [58] H. J. Arditty and H. C. Lefèvre, Sagnac effect in fiber gyroscopes, *Optics Letters* **6**, 401 (1981).
- [59] H. Barzegar, P. T. Chruściel, and E. Steininger, On elastic deformations of cylindrical bodies under the influence of the gravitational field, *Open Res. Europe* **4**, 10.12688/openreseurope.17329.2 (2024), arXiv:2401.16949 [gr-qc].
- [60] C. W. Misner, K. S. Throne, and J. A. Wheeler, *Gravitation* (W. H. Freeman, 1973).
- [61] F. W. J. Olver, in *Handbook of Mathematical Functions With Formulas, Graphs, and Mathematical Tables*, National Bureau of Standards Applied Mathematics Series No. 55, edited by M. Abramowitz and I. A. Stegun (United States Department of Commerce, 1972) Chap. 9. Bessel Function of Integer Order, pp. 355–433.
- [62] L.-Y. Chen, N. Goldenfeld, and Y. Oono, Renormalization group theory for global asymptotic analysis, *Phys. Rev. Lett.* **73**, 1311 (1994), arXiv:cond-mat/9407024.
- [63] L.-Y. Chen, N. Goldenfeld, and Y. Oono, Renormalization group and singular perturbations: Multiple scales, boundary layers, and reductive perturbation theory, *Phys. Rev. E* **54**, 376 (1996), arXiv:hep-th/9506161.